Observation of Alfvén Ion-Cyclotron Fluctuations in the End-Cell Plasma in the Tandem Mirror Experiment

T. A. Casper and Gary R. Smith
Lawrence Livermore National Laboratory, University of California, Livermore, California 94550
(Received 18 January 1982)

Ion-cyclotron fluctuations in the tandem mirror experiment have wave characteristics consistent with the Alfvén ion-cyclotron instability. The oscillations are coherent, have small azimuthal mode numbers, and have frequencies as low as 12% below the diamagnetically depressed, minimum ion-cyclotron frequency in the end cell. Polarization is in the direction of ion gyration, and azimuthal propagation is in either the electron or the ion diamagnetic direction, with the former prevailing.

PACS numbers: 52.35.-g, 52.55.Ke

The Alfvén ion-cyclotron (AIC) instability has been the subject of numerous theoretical studies[1-9] because it constrains the parameters of magnetic-mirror plasma-confinement devices. It is an electromagnetic instability that propagates principally along magnetic-field lines and that occurs in a plasma of sufficiently high anisotropy (ratio of mean perpendicular and parallel ion energies) and β (ratio of ion pressure to magnetic-field pressure). Evidence for the AIC instability in the plasma of Earth's magnetosphere has been presented.[10] However, ion-cyclotron fluctuations in magnetic-mirror devices, particularly in 2XII,[11] 2XII*B*,[2] and PR-6,[13] have been identified as the different drift-cyclotron loss-cone (DCLC) instability.[14]

In this paper we present evidence for the first definitive observation of the AIC instability in a laboratory plasma. The plasma was produced in the end cells of the tandem mirror experiment (TMX) by injecting neutral beams nearly perpendicularly to magnetic-field lines of the minimum-*B* mirror field.[15] When the instability was strong, plasma confinement was degraded.[16] Future experiments will also employ neutral-beam injection, but greater pitch-angle scattering and flexibility of the injection geometry will lessen the possibility of instabilities like AIC.[17,18] Our detailed study of the end-cell instability in TMX demonstrates the importance of injection geometry and helps to ensure the successful operation of the future experiments, which will be important elements in the quest for controlled thermonuclear fusion.

Disparity in the plasma parameters for 2XII*B* and the end cells of TMX made the AIC instability prevalent in TMX while the DCLC instability prevailed in 2XII*B*. The DCLC mode was strong in 2XII*B* because a_i/R_p was relatively large. Here, a_i is the ion (deuteron) gyroradius and R_p is the plasma radius. A comparison of the two experiments is shown as Table I, which gives nominal values of parameters affecting stability, including a_i/R_p. There is considerable variance of some parameters about the nominal values because of diverse operating conditions and shot-to-shot variability.

The AIC mode was strong in TMX because the parameter βA^2, which governs AIC stability, was large. Here, the anisotropy A is $\langle W_\perp\rangle/\langle W_\parallel\rangle$, where angular brackets denote an average over the velocity distribution of ions, and $W_\perp$ and $W_\parallel$ are perpendicular and parallel kinetic energies, evaluated at the point of minimum magnetic-field strength B_0 along a field line. Theoretical calculations[9] suggest that the AIC instability occurs if $\beta A^2 \gtrsim 8$ for a value of a_i/R_p close to that in 2XII*B*. For smaller a_i/R_p, as in TMX, instability occurs at values of βA^2 even lower than 8.[9] As shown in Table I, 2XII*B* was nominally at the AIC stability limit, while TMX was definitely unstable.

Among the 2XII*B* data, there exist ion-cyclotron fluctuations with small azimuthal mode

TABLE I. Parameters affecting stability.

Parameter	2XII*B*	TMX
a_i/R_p	0.37	0.13
β	0.33	0.07
$A \equiv \langle W_\perp\rangle / \langle W_\parallel\rangle$	5	14
βA^2	8	14
E_i (keV)	13	8
f_{ci0} (MHz)	4.9	7.6
R_p (cm)	7	10
L_p (cm)	25	16
L_v (cm)	75	50
L_m (cm)	39	43

number or with propagation in the electron diamagnetic direction.[12,19] These phenomena occur when either a_i/R_p or β or both are low and thus most similar to a_i/R_p and β in TMX. No instability other than DCLC was identified in 2XIIB though.

We calculate the anisotropy A in the two experiments from knowledge of the axial profiles of pressure and vacuum magnetic field. The anisotropy A is approximately $2(L_m/L_p)^2 = 2(1-\beta)[(\beta/2)+(L_p/L_v)^2]^{-1}$, in which we use the long, thin (or paraxial) approximation[20] to relate the axial scale lengths of plasma pressure (L_p), vacuum magnetic field (L_v), and actual field (L_m). Compared to 2XIIB, the TMX end-cell plasmas had a much lower β and therefore a less deep diamagnetic well and larger A, as seen in Table I.

At the midplane of the TMX end cells, we observed ion-cyclotron fluctuations with two types of probe arrays, one sensitive to electrostatic fields, the other to magnetic fields. In a spatially finite plasma, each type of probe can detect both AIC and DCLC instabilities. The array sensitive to electrostatic fields consists of five probe tips, each of which is a 0.1-cm-diam tungsten wire, 1 cm in length, terminated with a 10-kΩ resistor. This high-impedance probe is sensitive to floating-potential fluctuations $\tilde{\varphi}$ up to a frequency of at least 20 MHz. The 1-cm separation between probe tips allows the unambiguous resolution of wavelengths greater than 2 cm. Generally, the array was oriented to measure azimuthal wave numbers. In close proximity to the five-tip probe array, we used a probe consisting of three orthogonal, interwoven loops to measure radial, azimuthal, and axial components $\dot{B}_r$, $\dot{B}_\theta$, and $\dot{B}_z$ of the time derivative of the magnetic field. Observations were limited to radii $\geq 2R_p$, because insertion of probes farther into the plasma perturbed it significantly. All data presented here were taken in the "east" end cell of TMX. Data from the two end cells differ somewhat as a result of east-west asymmetries in TMX.

Digital time-series data from both types of probes are Fourier analyzed to determine the cross power spectral densities[21] $P_{12}(f) = |P_{12}(f)| \times \exp[i\theta_{12}(f)]$. The cross amplitude spectra $|P_{12}(f)|$ provide the power spectral content (in volts squared per hertz) of the time-series data. A coherent oscillation appears as a narrow maximum of $|P_{12}(f)|$ at the mode frequency f_0. The phase spectrum $\theta_{12}(f)$ is the relative phase between the signals on two probes, labeled 1 and 2, and is well defined only over regions of significant mode power. For the spatially separated $\tilde{\varphi}$ probes, the phase spectrum is proportional to the wave vector $\vec{k}$, with $\theta_{12}(f_0) = \vec{k}(f_0) \cdot \Delta\vec{r}$ for probe separation $\Delta\vec{r}$. For azimuthally propagating modes, $k = m/r_p$, where m is the azimuthal mode number and r_p is the radial position of the probe. The sign of $\theta_{12}(f_0)$ gives the direction of mode propagation. The phases at $f = f_0$ of the cross spectra between the orthogonal loop probes are the relative phases between the $\vec{B}$ components and provide the polarization of the wave.

The amplitude spectrum of potential fluctuations plotted in Fig. 1 is typical of TMX end-cell data.

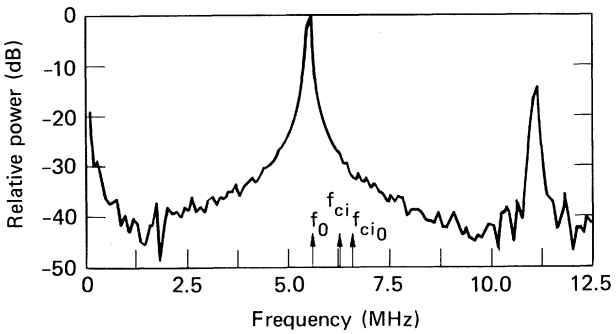

FIG. 1. Cross amplitude spectrum for potential fluctuations in the east TMX end cell. The narrow-band peak at $f_0 = 5.6$ MHz is due to instability-produced coherent oscillations.

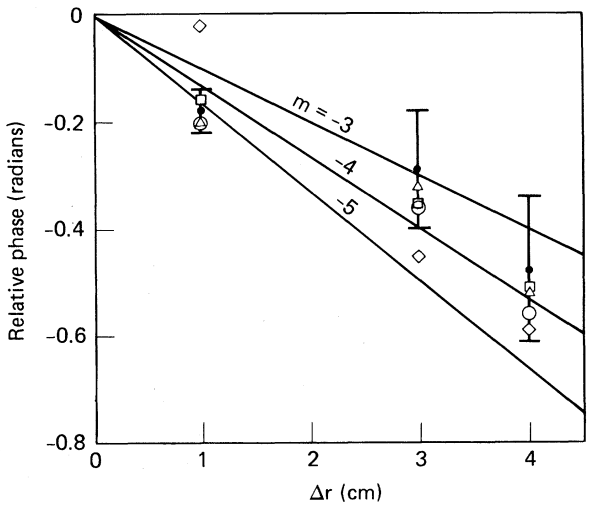

FIG. 2. Phase variation vs probe separation for fluctuations in the east TMX end cell. The symbols correspond to five different shots with single-shot error bars indicated; three of five tips were monitored. The inferred azimuthal mode number is $m = -4 \pm 1$.

The power spectrum obtained from a single probe tip is identical to the cross amplitude spectrum, indicating that the fluctuations are spatially homogeneous. The well-defined peak at $f_0 = 5.6$ MHz reveals the presence of a coherent oscillation with a frequency considerably below the vacuum ion-cyclotron frequency $f_{ci0} = 6.6$ MHz at the center of the end cell during this shot (87% of maximum field used). The observed oscillation frequency is roughly 12% below the actual cyclotron frequency $f_{ci} \approx 6.3$ MHz, estimated from the paraxial diamagnetic-depression factor $(1-\beta)^{1/2}$ with $\beta \approx 8.5\%$. Since the field geometry is minimum B and plasma parameters peak at the center of the end cell, f_0 is below the minimum cyclotron frequency in the end cell. Also, as expected for the AIC mode, $f_0 < f_{ci}(1 - \langle W_\parallel \rangle / \langle W_\perp \rangle)$. The phase spectrum for this shot yields a mode number $m = -2 \pm 1$. A negative m indicates propagation in the electron diamagnetic direction.

In Fig. 2 we plot the phase shifts recorded at f_0 versus probe separation for five shots with experimental conditions held approximately constant. The linear relation between phase shift and probe separation indicates that a single wave number is present. From Fig. 2 and $r_p = 30$ cm, we obtain an azimuthal mode number $m = -4 \pm 1$. The average oscillation frequency for these data is $f_0 = 7.0$ MHz, which is 5% below $f_{ci} = 7.4$ MHz. We observe $|m|$ as high as 6. Although propagation is generally in the electron diamagnetic direction, ion diamagnetic propagation is sometimes observed.

When the $\tilde{\varphi}$ probes are oriented to measure axial rather than azimuthal wave number, phase shifts are not statistically different from zero. Assuming that the fluctuations are not standing waves, we find a rough upper limit to the parallel wave number of 0.1 cm^{-1}.

We consider now the magnetic-field fluctuations. The power spectrum for each field component near f_0 is nearly identical to that shown for the potential fluctuations in Fig. 1. From the appropriate phase spectrum, we observe that $\dot{B}_r$ and $\dot{B}_\theta$ are about $-70°$ out of phase, with the minus sign indicating rotation of the $\vec{B}$ vector in the direction of ion gyration (a "left" polarized wave). The amplitude of axial magnetic-field fluctuations at f_0 is more than an order of magnitude less than either the radial or the azimuthal components. These results are consistent with an Alfvén wave. In Fig. 3 we plot $V_r(t)$ versus $V_\theta(t)$, the loop-probe voltages induced by $\dot{B}_r(t)$ and $\dot{B}_\theta(t)$, respectively. Digital filtering with a

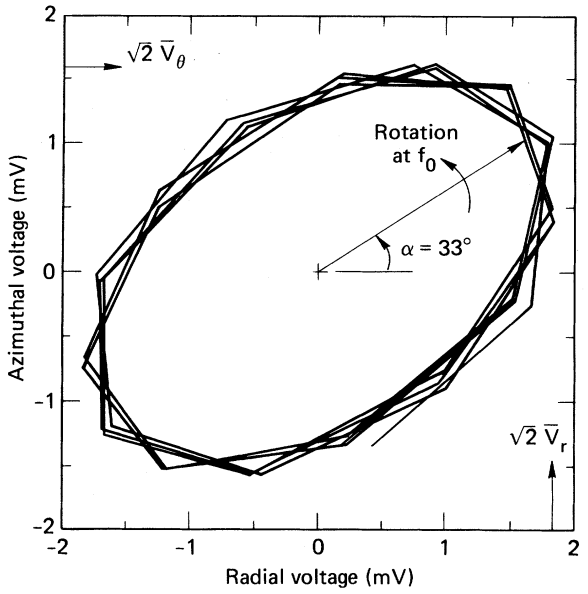

FIG. 3. Azimuthal vs radial induced loop voltages. The field vector rotates in the direction of ion gyration. The tilt angle of the ellipse indicates a $-65°$ phase shift between B_r and B_θ (i.e., an elliptically polarized wave).

3-MHz pass band about f_0 was used to remove low-frequency fluctuations and the harmonics of f_0. The tip of the total perpendicular field vector $\vec{B}_\perp(t) = B_r(t)\hat{r} + B_\theta(t)\hat{\theta}$ rotates in the direction of ion gyration (counterclockwise). The rms amplitudes are $\bar{V}_r = 1.33$ mV and $\bar{V}_\theta = 1.10$ mV; inequality of these rms amplitudes means that the wave is elliptically polarized. Alfvén waves propagating in finite-width plasmas have a polarization dependent upon the radial position of observation[22]; thus, noncircular polarization is not surprising. The tilt angle α of the ellipse in Fig. 3 is approximately 33°. This provides a second determination of the phase angle ξ between $\dot{B}_r$ and $\dot{B}_\theta$ as given by $\xi = \cos^{-1}[(\bar{V}_r{}^2 - \bar{V}_\theta{}^2)\tan(2\alpha)/2\bar{V}_r\bar{V}_\theta] = -65°$, which is consistent with the phase-spectrum measurement.

These induced voltages indicate an rms magnetic-field fluctuation of 2.7 mG at $r_p = 20$ cm. The magnitude of the fluctuations, both magnetic and electrostatic, is a strong function of radial position. Probe signals decrease by nearly an order of magnitude when we vary r_p from 20 to 30 cm. The rms floating potential at $r_p = 20$ cm is $\bar{\varphi} = 2$ mV.

In summary, probes measuring potential fluctuations show the presence of waves having small mode numbers $|m| \approx 4$ propagating in the electron diamagnetic direction. The oscillation frequency

can be significantly (12%) below the diamagnetically depressed ion-cyclotron frequency. Magnetic-fluctuation probes show that the mode is nearly left-circularly polarized. These characteristics are all consistent with an Alfvén-like wave generated by the AIC instability. Small m and left-circular polarization are inconsistent with the properties of the DCLC mode.

This work was possible only because of strenous efforts by numerous experimentalists and theorists on behalf of TMX. Particularly important were the contributions of D. P. Grubb, T. C. Simonen, and B. W. Stallard. We wish to thank the TMX computer programming staff and Gary Friedman in particular for their help. This work was performed under the auspices of the U. S. Department of Energy by the Lawrence Livermore National Laboratory under Contract No. W-7405-ENG-48.

[1]M. N. Rosenbluth, Bull. Am. Phys. Soc., Ser. II, 4, 197 (1959). See E. G. Harris, in U. S. Atomic Energy Commission Report No. TIO-7582, Proceedings of a Conference on Theoretical Aspects of Controlled Fusion Research, Gatlinburg, Tennessee, 1959 (unpublished), p. 133.

[2]J. Scharer, Plasma Phys. 11, 1 (1969).

[3]J. G. Cordey and R. J. Hastie, Phys. Fluids 15, 2291 (1972).

[4]A. Hasegawa, *Plasma Instabilities and Nonlinear Effects* (Springer-Verlag, New York, 1975), pp. 79–82.

[5]R. C. Davidson and J. M. Ogden, Phys. Fluids 18, 1045 (1975).

[6]T. D. Rognlien and D. C. Watson, Phys. Fluids 22, 1958 (1979).

[7]T. Tajima and K. Mima, Phys. Fluids 23, 577 (1980).

[8]T. Tajima and J. M. Dawson, Nucl. Fusion 20, 1129 (1980).

[9]D. C. Watson, Phys. Fluids 23, 2485 (1980).

[10]B. H. Mauk and R. L. McPherron, Phys. Fluids 23, 2111 (1980).

[11]T. C. Simonen, Phys. Fluids 19, 1365 (1976).

[12]W. C. Turner, J. Phys. (Paris), Colloq. 38, C6-121 (1977).

[13]B. I. Kanaev, Nucl. Fusion 19, 347 (1979).

[14]R. F. Post and M. N. Rosenbluth, Phys. Fluids 9, 730 (1966).

[15]T. C. Simonen *et al.*, in *Proceedings of the Eighth International Conference on Plasma Physics and Controlled Nuclear Fusion Research, Brussels, Belgium, 1980* (International Atomic Energy Agency, Vienna, 1981), Vol. I, p. 97.

[16]R. P. Drake *et al.*, Nucl. Fusion 21, 359 (1981).

[17]D. E. Baldwin, in Lawrence Livermore National Laboratory Report No. UCID-18496-Part 1, edited by D. E. Baldwin, B. G. Logan, and T. C. Simonen, 1980 (unpublished), p. I-28.

[18]F. H. Coensgen *et al.*, Lawrence Livermore National Laboratory Report No. LLL-PROP-172, 1980 (unpublished).

[19]B. I. Cohen *et al.*, in *Proceedings of the Eighth International Conference on Plasma Physics and Controlled Nuclear Fusion Research, Brussels, Belgium, 1980* (International Atomic Energy Agency, Vienna, 1981), Vol. I, p. 521.

[20]H. P. Furth and M. N. Rosenbluth, Phys. Fluids 7, 764 (1964).

[21]D. E. Smith, E. J. Powers, and G. S. Caldwell, IEEE Trans. Plasma Sci. 2, 261 (1974).

[22]J. A. Lehane and F. J. Paoloni, Plasma Phys. 15, 475 (1973).

Effect of Laser Wavelength and Pulse Duration on Laser-Light Absorption and Back Reflection

C. Garban-Labaune, E. Fabre, C. E. Max,[a] R. Fabbro, F. Amiranoff, J. Virmont, M. Weinfeld, and A. Michard

Equipe du GRECO Interaction Laser-Matière, Laboratoire de Physique des Milieux Ionisés, Groupe de Recherche du Centre National de la Recherche Scientifique, Ecole Polytechnique, F-91128 Palaiseau, France

(Received 17 August 1981)

Absorption efficiency has been measured in laser-irradiated plane-target experiments with various laser wavelengths (1.06, 0.53, and 0.26 μm), pulse durations (100 ps, 2 ns), and intensities (10^{10}–2×10^{15} W/cm). Results show a strong increase of absorption for long pulses, low intensities, and short wavelengths which favor inverse bremsstrahlung absorption. A one-dimensional Lagrangian hydrocode (FILM) is used to interpret these results.

PACS numbers: 52.50.Jm

High-gain targets for laser fusion applications require favorable performance in two areas of laser-plasma interaction physics: first, obtaining the highest absorption rate, and second, minimizing the generation of suprathermal electrons, especially considering their energy dis-